Korean J. Chem. Eng., 36(5), 650-659 (2019)
DOI: 10.1007/s11814-019-0257-3

pISSN: 0256-1115
eISSN: 1975-7220

Influence of cerium and cesium promoters on vanadium catalyst for sulfur dioxide oxidation

Xin Wang, Yong Kang†, Jie Li, and Dan Li

School of Chemical Engineering and Technology, Tianjin University, Tianjin 300350, China
(*Received 14 December 2018 • accepted 23 March 2019*)

Abstract−We studied the catalytic performance of vanadium catalyst promoted with cerium and cesium for sulfur dioxide oxidation. The catalyst samples were characterized by FT-IR, Raman, XRD, SEM, BET and XPS. The results showed that the properties of the catalyst promoted with 4 wt% CeO_2 and 7 wt% Cs_2SO_4 were superior to the commercial V_2O_5-K_2SO_4/SiO_2 and V_2O_5-K_2SO_4-Cs_2SO_4/SiO_2 catalysts, in terms of low temperature activity, thermal stability, SO_2 oxidation efficiency and ignition temperature. The FT-IR, Raman, XRD and XPS results evidenced the formation of V_2O_5-$Cs_2S_2O_7$ pyrosulfate, $CeVO_4$ and CeO_2 crystalline phase in V_2O_5-K_2SO_4-Cs_2SO_4-CeO_2/SiO_2 catalyst. These crystalline phases play an important role in redox reaction at low temperature and can increase the available oxygen for the redox reaction. The characterization results also showed that cerium can promote the formation of pyrosulfate, increase the proportion of large macropores, and improve stability of V^V at high temperature. Due to its excellent low-temperature and high-temperature activity, the V_2O_5-K_2SO_4-Cs_2SO_4-CeO_2 /SiO_2 catalyst appears to be more efficient for the conversion of SO_2 in a larger concentration range.

Keywords: Vanadium-cesium-cerium Catalyst, Sulfur Dioxide Oxidation, Catalytic Performance, Wide Temperature Catalyst, Ignition Temperature

INTRODUCTION

The sources of sulfur dioxide emission to the atmosphere include mainly sulfuric acid manufacture, smelting of nonferrous metals, coal-fired power generation and volcanic eruptions [1]. The catalytic oxidation of sulfur dioxide over the supported liquid phase catalyst is the key stage in the production of sulfuric acid [2]. Conventionally, the industrial catalyst used for this process is vanadium catalyst, which is made by calcination of diatomite, V_2O_5 and alkali promoters [3]. At the operation temperature about 400-600 °C, the reversible reaction of $V^V \leftrightarrow V^{IV}$ is continually performed as a reduction-oxidation reaction. The molecular structure of the species present during the reaction can be well described with the molten salt/gas system V_2O_5-$M_2S_2O_7$-M_2SO_4/SO_2-O_2-SO_3-N_2, where M is usually alkali metals (Na, K, Rb, Cs) [4].

Detailed investigations of the effect of the alkali metals (Na, K, Rb, Cs) showed that the activity of the V_2O_5 catalysts increased with the increase of the alkali atomic number, and the presence of Cs as a promoter improves the low-temperature activity with the ignition temperature decreasing below 400 °C [5]. The higher catalytic activity of Cs-V catalyst at low temperature can improve the economic benefits of sulfuric acid industry in turn [6].

With the implementation of the new pollutant discharge standards of sulfuric acid industrial and the increase of sulfur dioxide concentration in the tail gas of metallurgical plants and coal-fired power plants, the total amount of sulfuric acid produced by lower concentration and higher concentration of SO_2 makes up a large proportion of sulfuric acid preparation. So, it is necessary to handle such lower concentration and higher concentration of sulfur dioxide gas directly to gain cheaper construction and operation. However, the strong exothermicity during the reaction can lead to high temperatures, which would easily cause thermal breakdown and vanadium loss, resulting in pollution of the product acid [7]. In addition, low-temperature activity is also an essential part of sulfur dioxide oxidation in this case, since it would increase the adiabatic temperature range. To improve the conversion ratio of SO_2, development of the novel catalysts for sulfur dioxide oxidation in this case has become necessary from the economic and ecological point of view.

Due to the excellent properties of cerium oxide, some researchers have tried to utilize these oxides for the treatment of SO_2. Chen examined the catalytic reaction of SO_2 with CO over several metal oxide catalysts supported on the CeO_2 nanomaterial and found Cr_2O_3/nano-CeO_2 has the best catalytic performance [8]. Zhou studied the catalytic activity of cerium oxide cluster cations for the oxidation of SO_2 and found the bond strength of Ce-O and oxygen storage/release capacity of ceria are the key factors to the production of the SO_2 [9]. Xu prepared Pt/CeO_2/C composite catalysts and found the CeO_2 nanoparticles with very small size can offer the nucleation sites for Pt nanoparticle formation, effectively decreasing the average size, improving the dispersion of Pt nanoparticles and enhancing the SO_2 catalytic activity of Pt catalyst[10]. Mazidia studied the V_2O_5 catalyst promoted by ceria at temperature from 410 to 570 °C and found 7 wt% load of the ceria can lead to maximum catalyst activity [11]. Mathieu showed that an MCM-41 sorbent containing two metal oxides (CuO, CeO_2) and an alkaline additive (LiCl) had a high adsorption capacity of 130 mg SO_2/g and found cerium oxide partially oxidized SO_2 into SO_3 during the adsorption pro-

†To whom correspondence should be addressed.
E-mail: ykang@tju.edu.cn

cess [12]. These researches all show that ceria can be a potential promoter in sulfuric acid preparation.

In this study, the V_2O_5 catalyst system was doped with cerium and cesium to develop a wide-temperature catalyst for sulfuric acid production whose ignition temperature is lower and operating temperature range is wide. The effects of cerium and cesium on the structure property and the activity of V_2O_5 catalysts at low temperature and high temperature were also emphasized. The as-prepared catalysts were characterized by FT-IR, Raman, BET, XRD, SEM and XPS and the roles of cerium and cesium promoter on the catalyst performance were justified by the characterization results.

EXPERIMENTAL

1. Catalyst Synthesis

All catalysts investigated were prepared by ultrasonic mixing method using V_2O_5, H_2SO_4, and KOH, as well as $Ce(NO_3)_3{\cdot}6H_2O$ and Cs_2SO_4 as precursors and diatomaceous earth as the support material [11,13]. In a typical synthesis, a total of 7.00 g V_2O_5 was introduced stepwise into a solution of 12.95 g KOH (K/V=3/1) in 30 ml distilled water during 30 min. After filtration, the solution was heated to 40 °C under vigorous stirring and 9.90 g H_2SO_4 was slowly added. 10.10 g $Ce(NO_3)_3{\cdot}6H_2O$ and 7.00 g Cs_2SO_4 were dissolved in deionized water and impregnated in the orange-brown solid under vigorous stirring. The mixture was further stirred for 2 h at 40 °C and then mixed with 61.94 g diatomite in a kollermill for 3 h. TBL-2 catalyst extruder was used to extrude the paste into a cylindrical rod of Φ5 mm×(6.0-6.5) mm after 30 minutes of ultrasonic treatment. The cylindrical rods were dried at 110 °C for 1.5 h and were calcined at 550 °C for 3 h. The prepared sample contained 7 wt% V_2O_5, 20 wt% K_2SO_4, 7 wt% Cs_2SO_4 and 4 wt% CeO_2. Other samples were also prepared by the same procedure except the amount of $Ce(NO_3)_3{\cdot}6H_2O$ and Cs_2SO_4.

2. Catalytic Performance

According to the method described in the Chinese Chemical Industry Standard HG/T 2089-2007 (*Test method of activity for oxidizing sulfuric dioxide into sulfuric acid catalyst*), the activity measurement was carried out in a 32 mm i.d. fixed bed stainless steel tube microreactor [14]. The height of catalyst bed was about 38 mm. The catalysts with the mesh size of 4-6 mm were loaded into the microreactor. At atmospheric pressure, the commercial feed gas (10±0.1% SO_2 (99.98%) and 90% air) with the gas hourly space velocity (GHSV) of 3,600 h^{-1} was used in the catalytic activity tests. All gases were dried through P2O5 columns. The feed gas concentration and velocity remained constant in all tests.

The exothermic reversible reaction $SO_2+1/2O_2=SO_3$ was carried out in the whole liquid volume dispersed on the surface of the carrier. Active pyrosulfate-containing molten salt $V^V_2O_4(SO_4)_2S_2O_7^{4-}$ forming during catalyst activation is the key to high catalytic activity. The performance of the catalyst was tested at 310-570 °C and was calculated according to the concentration change between inlet and outlet of the reactor measured by iodometry method. SO_2 Conversion is defined as the following Eq. (1):

$$E=\frac{(\phi_1-\phi_2)}{\phi_1(1-0.015\phi_1)} \quad (1)$$

where ϕ_1 is inlet volume fraction of SO_2 and ϕ_2 is outlet volume fraction of SO_2.

3. Catalyst Characterization

The BET surface area and the pore size distribution of the catalyst samples were measured at −196 °C in an AUTOSORB-iQ2-MP apparatus by N_2 adsorption and desorption. Before the experiments, the samples were treated under vacuum at 300 °C for 1 h to remove moisture from the surface. FT-IR of KBr pellets was performed by an AVATAR 370 Thermo Nicolet spectrophotometer in a scanning range of 400 cm^{-1} to 4,000 cm^{-1} taking scan number of 32 with a resolution of 2 cm^{-1}. Raman spectra were measured by Renishaw in Via with 532 nm Nd : YAG laser as excitation source. The Raman spectra were collected in the range of 50-1,500 cm^{-1} with a resolution of 1 cm^{-1}. To study the structure and crystallinity of the samples, XRD was carried out by Rigaku D/max 2500 diffractometer in the 2θ scan range of 5-80°, using the radiation of Cu Kα (λ=0.15405 nm, step size 0.02°). Surface morphology of the catalysts was studied by field-emission scanning electron microscope (FESEM, Hitachi S-4800). Elemental analysis was performed by EDX (NORAN-System7, Thermo Fisher Scientific, USA). X-ray photo-electron spectroscopy (XPS) spectra of the catalyst were performed using a Thermo ESCALAB 250 with Al Kα (hv=1,486.8 eV) as the excitation source. The binding energies were calibrated using C 1s peak of contaminant carbon (284.6 eV) as standard.

RESULTS AND DISCUSSION

1. Catalytic Performance

Fig. 1 shows the catalytic performance for the oxidation of SO_2 over the catalyst samples with different content of CeO_2. Catalytic performance is given as a percentage of SO_2 conversion. Generally, the trends of SO_2 conversion versus the content of CeO_2 promoter at most temperatures were similar, and the ceria loading of 4 wt% led to the maximum catalyst activity, showing that 4 wt% is the optimal content of CeO_2 in the catalyst. A certain amount of cerium

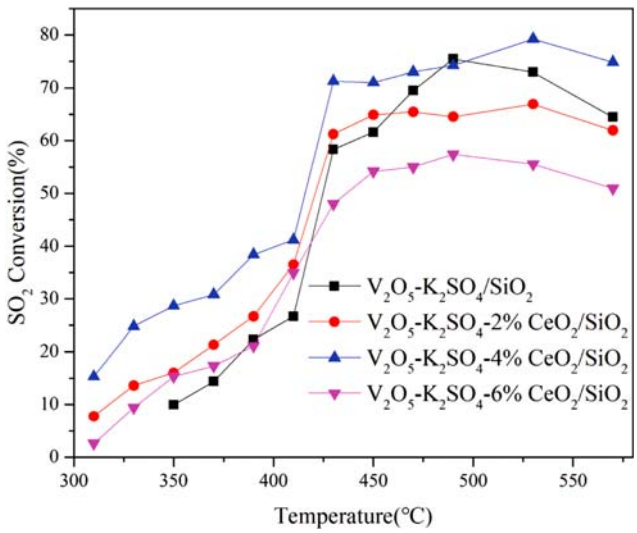

Fig. 1. Effect of CeO_2 addition on the catalytic performance of the V_2O_5-K_2SO_4/SiO_2 catalysts for SO_2 oxidation.

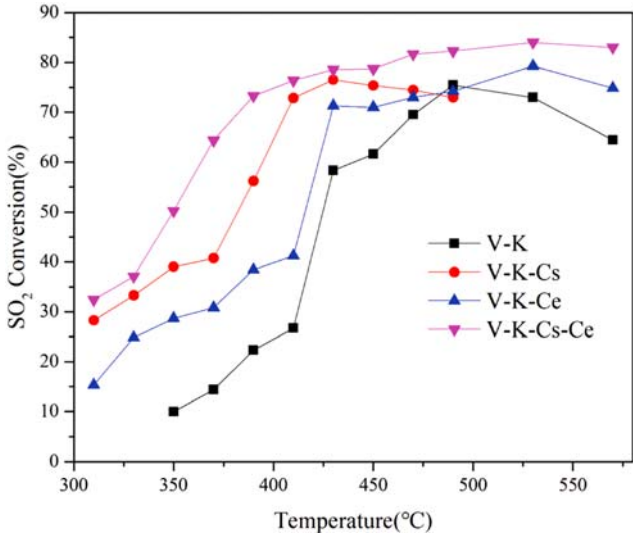

Fig. 2. Effect of cerium and cesium promoters on SO_2 conversion at various temperatures.

can promote the formation of pyrosulfate and cerium exists in the form of cerium oxide and $CeVO_4$, which can increase the available oxygen for the reaction. When the content of CeO_2 increases by more than 4%, the activity of catalyst decreases due to the pore blockage of diatomite carrier. Therefore, this sample (with ceria loading of 4 wt%) was selected for more investigation in this study.

The catalytic performance for the oxidation of SO_2 over V_2O_5-K_2SO_4/SiO_2 (V-K), V_2O_5-K_2SO_4-Cs_2SO_4/SiO_2 (V-K-Cs), V_2O_5-K_2SO_4-4%CeO_2/SiO_2 (V-K-Ce) and V_2O_5-K_2SO_4-Cs_2SO_4-4%CeO_2/SiO_2 (V-K-Cs-Ce) catalysts was compared at various temperatures between 310-570 °C as shown in Fig. 2. The catalyst of V_2O_5-K_2SO_4-Cs_2SO_4/SiO_2 contains 7 wt% Cs_2SO_4 which is the same as the commercial low temperature vanadium catalyst S107. The activity of all catalysts gradually increased with the increase of reaction temperature before deactivation and reduced after deactivation temperature. The results showed that SO_2 oxidation on V-K and V-K-Ce catalysts was ignited at 420 °C, and the ignition temperature of V-K-Cs and V-K-Cs-Ce catalysts was 380 °C and 340 °C, respectively. Addition of cerium in the cesium vanadium catalyst made the activity-temperature curve move about 40 °C towards low temperature, which may be attributed to the oxygen vacancies of ceria structural network and the formation of more pyrosulfate during the reaction.

Above the ignition temperature, the conversion of SO_2 over the V-K catalyst rose from 430 °C to 470 °C and fell from 490 °C to 530 °C. The activity reduction might result from the thermodynamic equilibrium limitation and the deactivation of V-K catalyst at high temperature. Although V-K-Cs catalyst showed a higher maximum catalytic activity compared with V-K catalyst, its performance at high temperature was even worse as shown in Fig. 2. The results demonstrated the significant effect of ceria loading on the high-temperature catalytic activity. It was obvious that with enhancing the ceria content of the V-K catalyst, the mean SO_2 conversion increased from 67.0% to 73.9% and the deactivation temperature rose from 490 °C to 530 °C. For the V-K-Cs-Ce catalyst, the trend of SO_2 conversion at high temperature was similar to that of V-K-Ce catalyst. At high temperature, V-K-Cs-Ce catalyst also showed highest catalytic activity compared with the other catalysts, and the mean conversion was about 79.7%.

When the temperature was lower than the ignition temperature, non-promoted V-K catalysts exhibited very low activities for SO_2 oxidation. However, the V_2O_5 catalysts promoted with Cs_2SO_4 and CeO_2 had a higher activity, which increased the mean SO_2 conversion from 18.3% to 35.3% and 29.8%, respectively. Interesting features were revealed from the low-temperature activity result of V-K-Cs-Ce catalyst and its mean conversion of SO_2 was not as high as expected, only slightly higher than that of V-K-Cs catalyst. It is because the textural properties decreased with the addition of both Cs_2SO_4 and CeO_2 and this will be discussed in SEM and BET parts.

Finally, the obtained results revealed that the V-K-Cs-Ce catalyst had the highest activity among other as-prepared catalysts in this work. Addition of CeO_2 can reduce deactivation of the catalysts at high temperature and the excellent stability results from reduction of $KV(SO_4)_2$ and the improvement of the thermal stability which will be discussed later. Furthermore, the low temperature performance of the catalyst including the ignition temperature and the SO_2 oxidation efficiency was also improved.

2. N_2 Adsorption/Desorption Analysis

The textural properties such as BET surface area and pore volume of the catalysts are summarized in Table 1. The V-K catalyst had the highest surface area of about 4.0 m^2/g. It can be observed that with the promoters addition in V_2O_5 catalyst, its BET surface areas decreased gradually. Remarkably, the specific surface area of V-K-Ce catalyst decreased not as obviously as that of Cs or Cs-Ce doping catalysts. The relatively smaller surface area loss of V-K-Ce catalyst might be due to the presence of small particles of CeO_2, the better dispersion of CeO_2 on the support, and the promotion of CeO_2 to the dispersion of the active component, to some extent. Furthermore, with the incorporation of cerium and cesium promoters in V_2O_5 catalyst, the pore volume of the V-K-Cs and V-K-Cs-Ce catalysts decreased slightly compared to that of the V-K catalyst. This could result from migration of promoters to the pores of the catalyst and clogging some pores by the addition of promot-

Table 1. Textural properties of the prepared catalyst samples with various components

Sample	Composition	BET (m^2/g)	Pore volume ($\times10^{-2}$ cm^3/g)
V-K	V_2O_5-K_2SO_4/SiO_2	4.0	1.14
V-K-Cs	V_2O_5-K_2SO_4-CeO_2/SiO_2	3.1	1.03
V-K-Ce	V_2O_5-K_2SO_4-Cs_2SO_4/SiO_2	3.7	1.32
V-K-Cs-Ce	V_2O_5-K_2SO_4-CeO_2-Cs_2SO_4/SiO_2	2.9	0.98

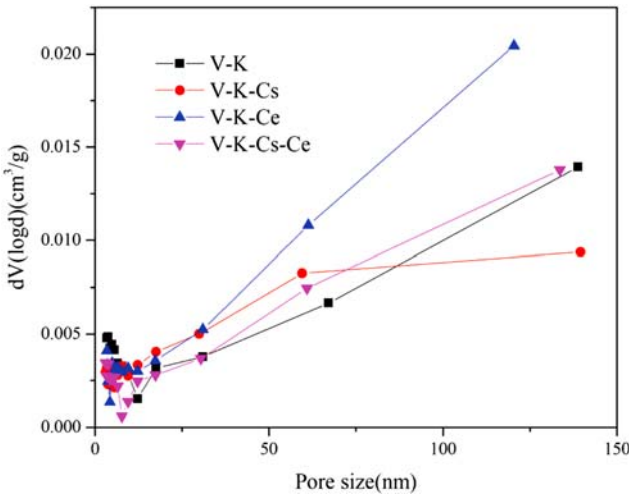

Fig. 3. Pore size distribution of the as-prepared catalysts.

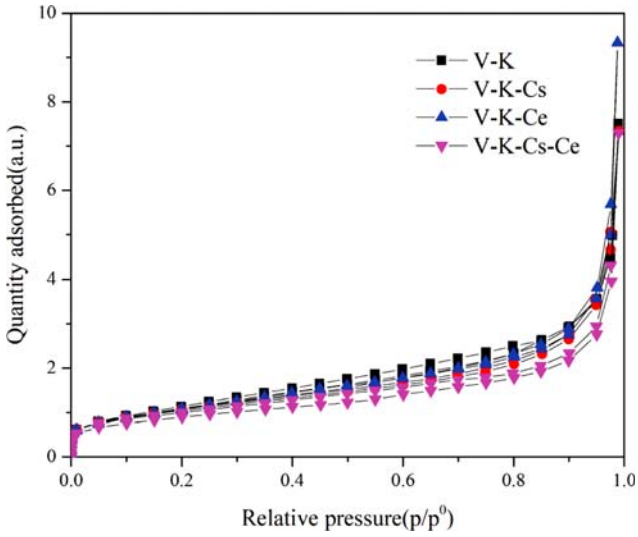

Fig. 4. Nitrogen adsorption-desorption isotherms of the catalysts.

ers into V_2O_5 catalyst, which might cause the reduction of pore size. However, the pore volumes of the cerium-promoted catalysts increased, which indicates that the cerium promoter can improve the thermal stability of diatomite and prevent the collapse of pore structure at high temperature [15].

Fig. 3 shows the pore size distributions (PSD) of the prepared catalysts. Both kinds of catalysts had a BJH pore-size distribution in the range of 0-150 nm, and it slightly shifted to smaller sizes with the addition of Cs promoter. In addition, PSD of V-K-Ce catalyst was excellent, and the order of PSDs was V-K-Ce>V-K-Cs-Ce>V-K>V-K>V-K-Cs. The addition of ceria shifted PSD to larger pore size, which might be attributed to the improvement of thermal stability. More importantly, the V-K-Ce catalyst had the highest proportion of large macropores, which was beneficial to the diffusion of SO_2. Although there was a sharp decrease in the proportion of large macropores, the V-K-Cs-Ce catalyst showed the best catalytic performance among all catalysts. It may be concluded

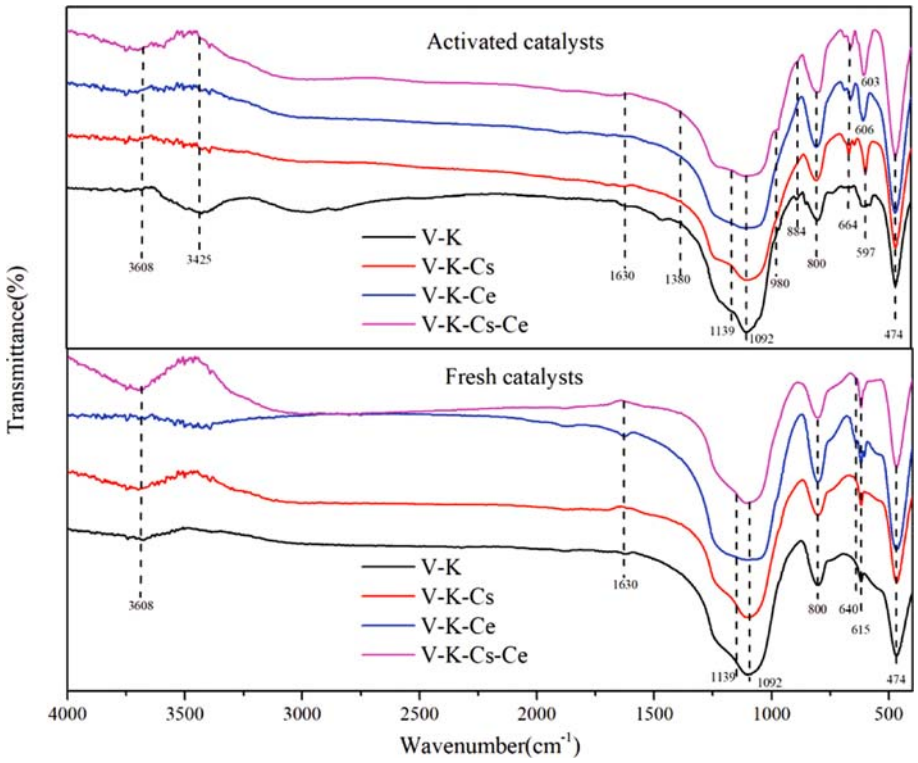

Fig. 5. FT-IR spectra of fresh catalysts calcined in air for 3 h and the ones after activation in [SO_2]=10 vol% for 2 h, GHSV=3,600 h^{-1}, P=107 kPa and T=25-470 °C.

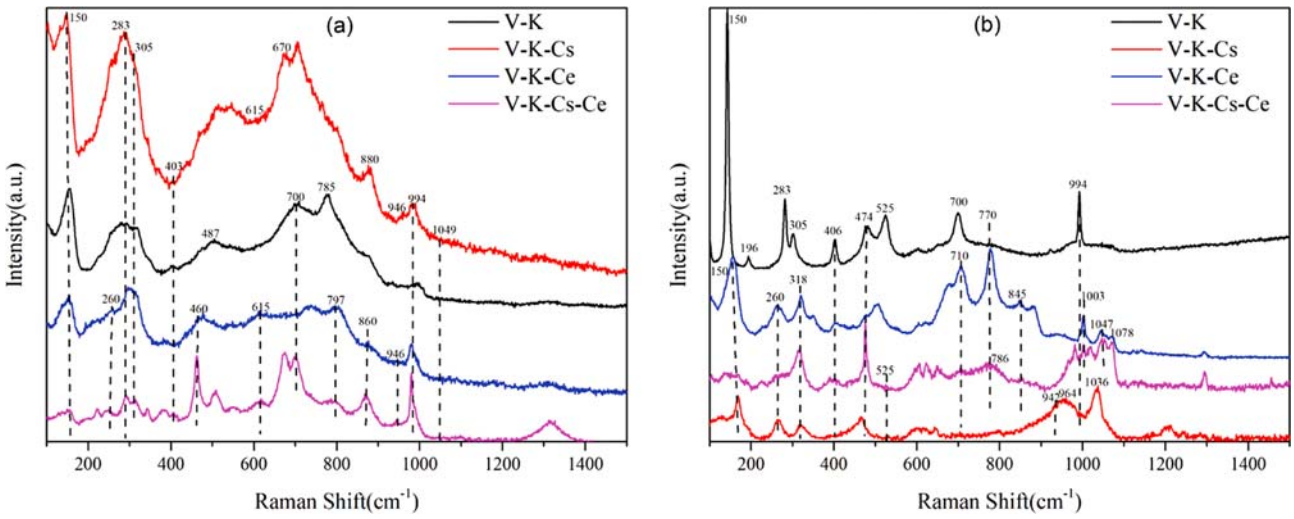

Fig. 6. Raman spectra of fresh catalysts (a) and the ones obtained after activation (b), respectively.

that the positive role of adding CeO_2 and Cs_2SO_4 to the catalyst can overcome the negative effect of decreasing the textural properties.

Fig. 4 shows the N_2 adsorption-desorption isotherms of the catalysts. These curves are similar to each other and can be identified as type II. According to the IUPAC classification, type II is characteristic of adsorption on macroporous adsorbents with strong adsorbate-adsorbent interactions. H3-type hysteresis loops were observed in all catalyst samples at about P/P^0=0.20-0.90, indicating the existence of the agglomerates of the particles with slit-shaped pores and non-uniform size [16]. Compared with other catalysts, the H3-type hysteresis loop of V-K-Cs-Ce catalyst occurred at a lower relative pressure (p/p^0), which was attributed to a smaller macropore in the sample [17].

3. FT-IR Characterization

FT-IR spectra of fresh catalysts calcined in air for 3 hours and those of catalysts activated by SO_2 and air is shown in Fig. 5. A large amount of adsorbed H_2O in the catalysts can be detected at 3,425 and 1,630 cm^{-1} bands, and the wide band at about 3,608 cm^{-1} may result from O-H stretching vibration of free H_2O in the environment [18]. All the spectra showed sharp and strong vibrational bands at 1,092 and 800 cm^{-1} due to the asymmetric and symmetric stretching modes of Si-O tetrahedral, respectively [19]. The other band around 474 cm^{-1} is attributed to the Si-O-Si bridges deformation [20]. The wide band between 1,250 and 1,000 cm^{-1} shows the adsorption of sulfur species on the surface of the catalyst [21]. The existence of sulfate group can be proved by the two bands at 1,139 and 615 cm^{-1} [22,23]. The more intense band at 800 cm^{-1} with a shoulder at around 737 cm^{-1} in fresh V-K-Ce and V-K-Cs-Ce catalysts is for the VO_4 units in the terms of orthovanadate [24]. The infrared spectrum of fresh V-K-Cs catalyst is almost the same as that of V-K catalyst. However, V-K-Ce and V-K-Cs-Ce catalysts showed a new band at about 640 cm^{-1} and an increase in the absorption at 615 cm^{-1} which may correspond the formation of SO_4^{2-} [23]. Eventually, these bands indicate that cesium promoter, like potassium, may exist in the form of sulfate and cerium may exist in the form of cerium vanadate and sulfate in the fresh catalysts.

For the activated catalysts, a small band displayed at 980 cm^{-1} can be assigned to the V=O stretch vibration of polymeric vanadyl species [25]. The bands at 1,380, 884 and 664 cm^{-1} originate from the formation of pyrosulfate $S_2O_7^{2-}$ [26]. The increase of the band at 664 cm^{-1} indicates that cerium can be beneficial to the formation of pyrosulfate, which may result in creation of active intermediates composed of sulfate and pyrosulfate complexes of vanadium compounds and increase the reaction rate of catalytic oxidation. Compared with fresh catalysts, the band at 615 cm^{-1} increases and shifts to lower wavenumber, which may be attributed to the transformation from $VO(SO_4)_2$ to $KV(SO_4)_2$ during SO_2 oxidation reaction. The minimum shift of the band to the lower wavenumber in V-K-Ce catalyst means there is a minimum formation of new catalytic inactive phases $KV(SO_4)_2$ [22].

4. Raman Characterization

Raman spectroscopy was used to discriminate different structures of vanadium catalysts because it can directly detect structures and bonds through its vibrational spectrum. Fig. 6 shows the Raman spectra of fresh catalysts and catalysts activated by sulfuric acid syngas, respectively. In Fig. 6(a), the bands at 150, 283, 305, 403, 700 and 994 cm^{-1} correspond to V_2O_5 orthorhombic phase [23]. Significantly, the bands at 487, 670, 785 and 1,049 cm^{-1} are known to originate from the presence of $(V^VO)_2O(SO_4)_4^{4-}$ complex [27]. The results of spectral comparison show that the spectra of the V-K-Cs, V-K-Ce and V-K-Cs-Ce catalysts have superposition bands at 946, 880 and 615 cm^{-1} due to the presence of V_2O_5-K_2SO_4 molten mixtures [28]. The characteristic band at 460 cm^{-1} can be assigned to the F2g mode of fluorite type cubic structure, which corresponds to the symmetric vibration of oxygen ions around Ce^{4+} ions in the cerium oxide [29]. The V-K-Ce and V-K-Cs-Ce catalysts present a series of characteristic sharp bands at 860, 797 and 260 cm^{-1} which are assigned to the $CeVO_4$ crystalline [30].

The Raman spectrum of activated V-K catalyst shows the characteristic bands of V_2O_5 at 150, 196, 283, 305, 403, 474, 525, 700 and 994 cm^{-1}. The weaker characteristic V_2O_5 bands and the shift of some bands in other samples indicate that V_2O_5 is low in crystallinity and has better dispersion [31]. In addition, a broad band at

964 cm^{-1} in V-K-Cs catalyst is very noticeable, which can be attributed to the V^{IV} complex $V^{IV}O(SO_4)_2^{2-}$ formed during reaction [6]. It is well established that below a certain temperature, $V^{IV}O(SO_4)_2^{2-}$ crystalline might be a plausible compounds which can lead to catalyst deactivation by depleting the active molten phase of vanadium [32]. This band became much weaker with adding cerium in V-K-Cs-Ce catalyst. The V-K-Ce and V-K-Cs-Ce catalysts present a series of characteristic bands for $CeVO_4$ crystalline, as discussed above. These two samples also present a feature at 710 cm^{-1} attributed to the V-O-Ce stretching mode, similar to cerium vanadate species [33]. A stronger band at 1,078 cm^{-1} due to the $\nu_1(S_2O_7^{2-})$ mode appears in V-K-Ce and V-K-Cs-Ce catalysts, indicating a slight excess of molten pyrosulfate [34]. Indeed, the superposition of bands of $V^VO_2(SO_4)_2^{3-}$ (1,036 and 942 cm^{-1}) appears in the spectrum of V-K-Cs catalyst. Characteristic bands at 1,047, 1,003, and 845/770 cm^{-1} in the spectrum of V-K-Ce and V-K-Cs-Ce catalyst correspond to $V_2^VO_4(SO_4)_2S_2O_7^{4-}$ and the bands of $V^VO_2(SO_4)_2^{3-}$ became weaker [35,36]. Thus, the addition of cerium into vanadium catalyst can promote the conversion of mononuclear $V^VO_2(SO_4)_2^{3-}$ to binuclear $V_2^VO_4(SO_4)_2S_2O_7^{4-}$ species, which is considered to be an active species in sulfur dioxide catalytic oxidation cycle of V_2O_5 catalyst [28,32].

5. XRD Characterization

Fig. 7 shows the XRD patterns of diatomite, fresh catalysts and activated catalysts. The XRD patterns of diatomite show a broad reflection at 20-25°, which is characteristic of amorphous silica phase, the diffraction peaks at 26.7° for the presence of quartz (SiO_2), diffraction peaks at 22.0, 24.1 and 28.1° correspond to albite ($Na(AlSi_3O_8)$) and diffraction peak at 35-36° corresponds to cristobalite, which was transformed from the amorphous silica phase at high temperature [37,38]. Due to the pretreatment of diatomite, no diffraction peaks of alumina and iron oxide appear on the XRD patterns [39].

The fresh V-K catalyst shows diffraction peaks at 21.3, 29.7, 30.8, 35.6, 37.1 and 43.3° for potassium sulfate (K_2SO_4, PDF No. 72-0354), diffraction peaks at 11.5, 25.7, 27.9, 29.8, 31.8 and 41.0° for potassium vanadium oxide (KV_3O_8, PDF No. 22-1247), and diffraction peaks at 12.4, 27.8, 28.4, 38.0, 40.6, 44.9 and 51.0° correspond to vanadium oxide (V_2O_5, PDF No. 53-0538). Compared with the fresh V-K catalyst, V-K-Cs catalyst shows new diffraction peaks at 25.3, 31.4, 32.0 and 40.6° due to the formation of cesium vanadium oxide ($Cs_2V_4O_{11}$, PDF No. 37-0105) and diffraction peaks at 19.7, 25.3, 27.6, 33.9, 37.9, 43.4 and 49.4° for cesium sulfate (Cs_2SO_4, PDF No. 21-0854). V-K-Ce catalyst shows the new diffraction peaks at 28.4, 33.0 and 47.5°, which is characteristic of cerium oxide (CeO_2, PDF No. 65-5923), diffraction peaks at 18.1, 24.0, 33.0, 34.3, 39.0, 43.5, 47.9, 49.2 and 55.6° for cerium vanadium oxide ($CeVO_4$, PDF No. 12-0757) and diffraction peaks at 11.5, 12.6, 13.8, 20.5, 23.5, 26.3, 28.4, 29.0, 29.8, 30.8, 32.6, 41.7, 43.9 and 47.2° correspond to potassium cerium sulfate ($K_8Ce_2(SO_4)_7$, PDF No. 39-0646). The XRD pattern of V-K-Cs-Ce catalyst shows all the new diffraction peaks mentioned in the V-K-Cs and V-K-Ce catalysts.

Compared to fresh V-K catalyst, the activated V-K catalyst shows new diffraction peaks at 11.3, 23.8, 31.3 and 49.9° for potassium vanadium sulfate ($KV(SO_4)_2$, PDF No. 25-0692), and diffraction peaks at 24.4, 25.4, 31.3, 38.1 and 39.7° correspond to potassium sulfate ($K_2S_2O_7$, PDF No. 22-1239). After activation, the diffraction peaks of K_2SO_4 and KV_3O_8 become weaker, which resulted from the conversion to $KV(SO_4)_2$ and $K_2S_2O_7$. Activated V-K-Cs catalyst shows diffraction peaks at 24.2, 25.2, 26.0, 27.8 and 37.8° for cesium vanadium oxide sulfate ($Cs_4V_2O_4(SO_4)_2S_2O_7$, PDF No. 36-0709), diffraction peaks at 11.7, 21.2, 23.7, 24.4, 27.0, 29.2, 37.8, 42.2 and 43.9° correspond to cesium vanadium oxide ($Cs_2V_6O_{16}$, PDF No.40-0456), diffraction peaks at 28.5, 32.2 and 37.5° correspond to cesium vanadium oxide sulfate ($Cs_3VO_2(SO_4)_2$, PDF No. 36-0707). V-K-Ce catalyst shows diffraction peaks at 10.4, 12.7, 16.0, 17.0, 19.2, 23.3, 25.6, 26.4, 27.0, 28.6, 30.4, 30.8, 32.7, 33.0 and 43.9° for potassium cerium sulfate ($KCe(SO_4)_3$, PDF No. 40-026), diffraction peaks at 26.3, 27.7, 27.9, 30.1, 32.0, 32.3, 39.6, 46.0, 46.1 and 46.3° for cerium oxide (Ce_6O_{11}, PDF No. 32-0196), diffraction peaks at 24.0, 39.0, 49.2 and 55.6° for cerium vanadium oxide

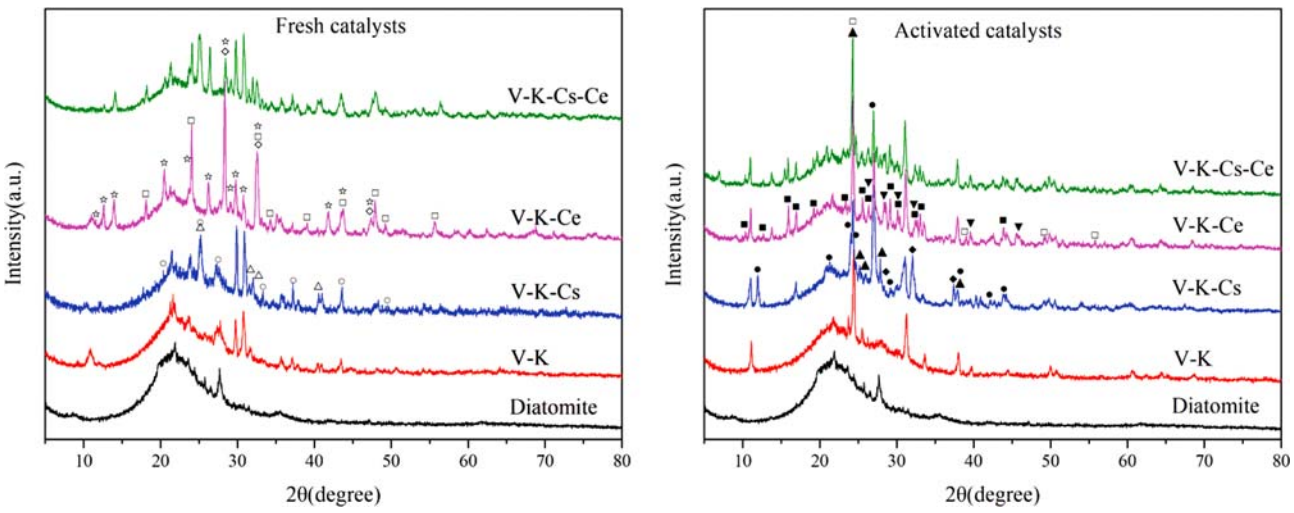

Fig. 7. XRD patterns of the fresh catalysts and the activated catalysts. Symbols: (△) $Cs_2V_4O_{11}$, (○) Cs_2SO_4, (◇) CeO_2, (□) $CeVO_4$, (☆) $K_8Ce_2(SO_4)_7$, (▲) $Cs_4V_2O_4(SO_4)_2S_2O_7$, (●) $Cs_2V_6O_{16}$, (◆) $Cs_3VO_2(SO_4)_2$, (■) $KCe(SO_4)_3$, (▼) Ce_6O_{11}.

($CeVO_4$, PDF No. 12-0757), more intense diffraction peaks for $K_2S_2O_7$ and do not show peaks for $KV(SO_4)_2$. V-K-Cs-Ce catalyst shows all the new diffraction peaks mentioned in the V-K-Cs and V-K-Ce catalysts except diffraction peaks for $KV(SO_4)_2$.

Consequently, adding cerium and cesium promoters into V_2O_5 catalyst has caused notable changes in the catalyst patterns. Cesium vanadium oxide and cesium sulfate were observed in V-K-Cs and V-K-Cs-Ce samples, which was related to cesium promoter. Cerium oxide, cerium vanadium oxide and potassium cerium sulfate were also seen in V-K-Ce and V-K-Cs-Ce samples, which was related to cerium promoter. The target component cesium sulfate transformed to active liquid phase pyrosulfate molten salt during the reaction. Adding cerium to catalyst can promote the formation of pyrosulfate, reduce the formation of the inactive low-value vanadium phase and the precipitation of V_2O_5 crystal phase.

6. SEM Micrographs

Fig. 8 shows the SEM micrographs of vanadium catalysts with different components. SEM micrographs of all the catalysts show a highly complex carrier structure with numerous fine microscopic pores, cavities and channels which correspond to the skeletons of diatoms. This diatomite mainly contains cylindrical straight-chain diatoms, which is the most ideal carrier for vanadium catalyst. The diameter of the cylinder was about 10-15 μm and was about 8-20 μm long, with a part of the cylinder having a central hole. Due to the load of the active component, the channels distributed on the outer wall of the cylinder were smaller than that of the channels described in literature [40,41]. After the addition of cerium promoter, the porous texture of diatomite still remains well compared with the V-K catalyst, which further confirmed the excellent dispersion of cerium and the improvement of thermal stability of diatomite as concluded in the BET part. However, adding cesium sulfate to the V_2O_5 catalyst clogged partial pores and reduced pore size, and the fragmentation of the diatomite also became more serious. Therefore, a considerable pore blockage can be seen in the SEM micrograph of V-K-Cs-Ce catalyst, which caused sharp decrease in BET area and pore volume, but the original geometry was mostly preserved because of the addition of cerium and the improvement of thermal stability under calcining temperature. The results of SEM analysis are consistent with those of BET.

Fig. 9 shows the coarse surface of V-K-Cs-Ce catalysts. It was observed that cerium and cesium promoters had excellent distributions on the V-K-Cs-Ce sample. The elemental mapping in Fig. 9 confirmed the joint existence of cesium, vanadium and oxygen, which were related to $CeVO_4$ and the existence of cerium, sulfur, potassium and oxygen, which might be related to $K_8Ce_2(SO_4)_7$. Also, the simultaneous existence of cesium, sulfur and oxygen could be related to cesium sulfate or cesium pyrosulfate. These results are consistent with those of XRD and FT-IR.

7. XPS Analysis

X-ray photoelectron spectroscopy (XPS) was used to characterize the inclusion of cerium and cesium promoter in the V-K-Cs-Ce catalyst and to study in more detail the changes in the nature of catalyst in the presence of Cs and Ce ions.

The O 1s peak at about 532.0 eV and the Si 2p peak at about 103.6 eV correspond to O and Si elements in diatomite, respectively [42]. Due to the formation of oxides of cerium and vana-

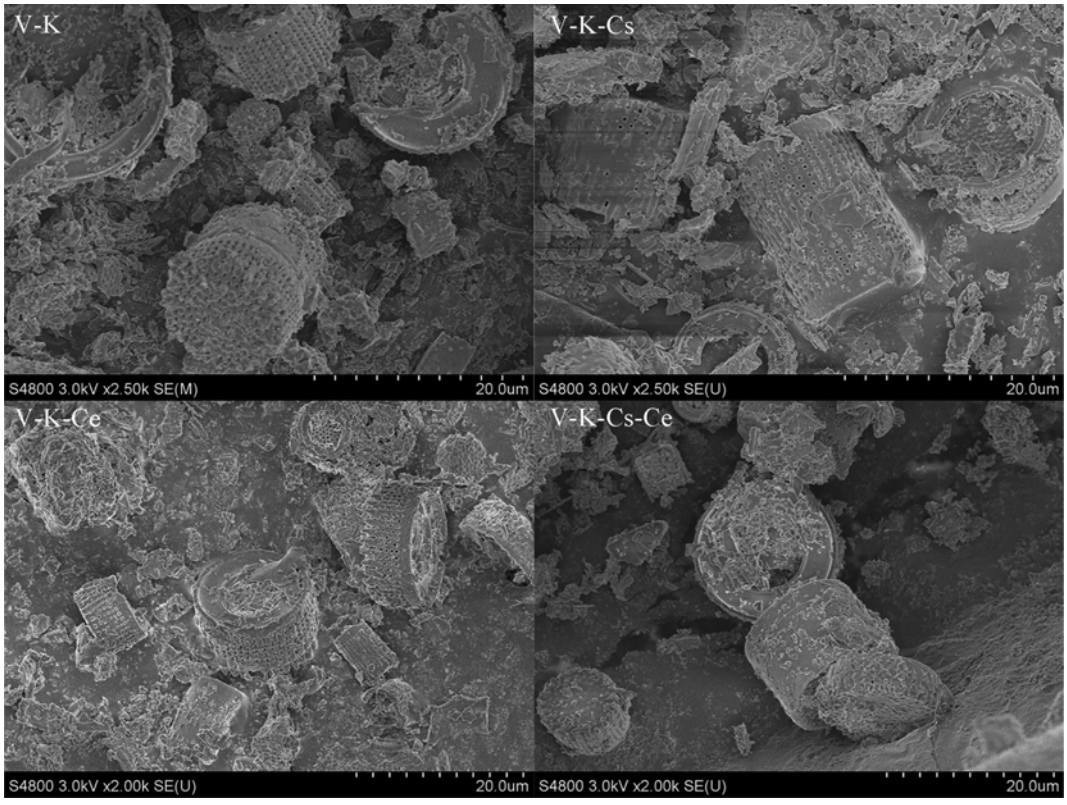

Fig. 8. SEM images of the prepared catalysts.

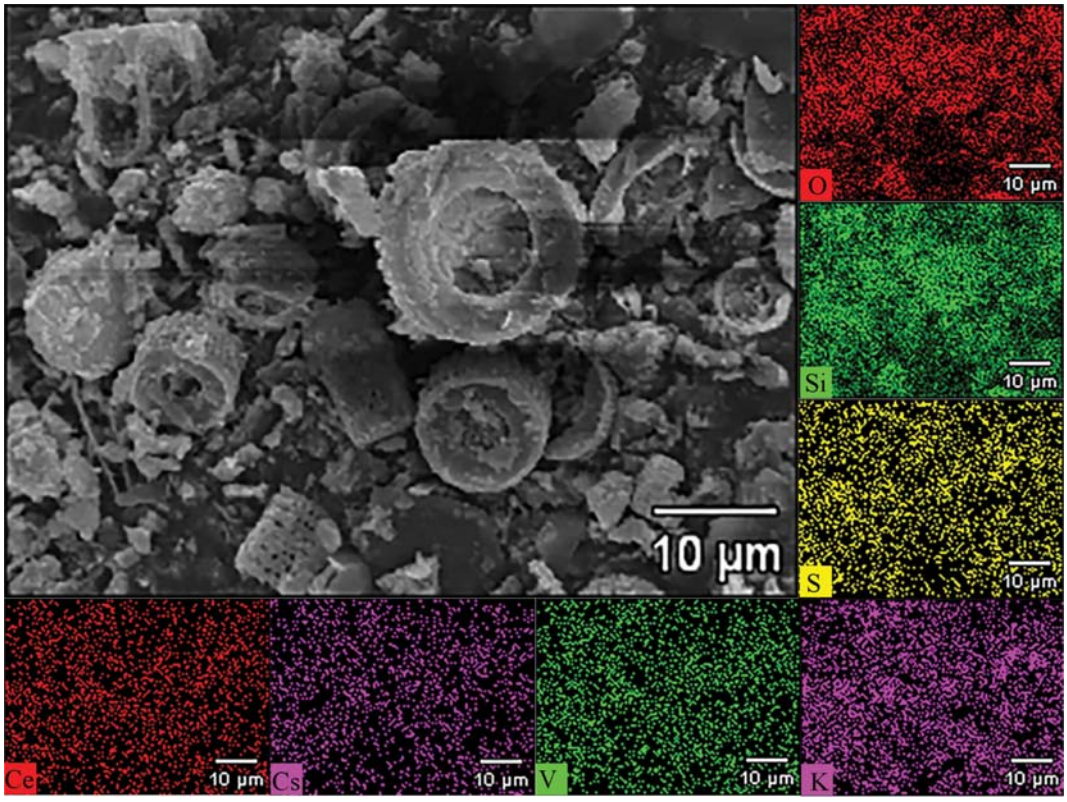

Fig. 9. SEM analysis of the V-K-Cs-Ce catalyst.

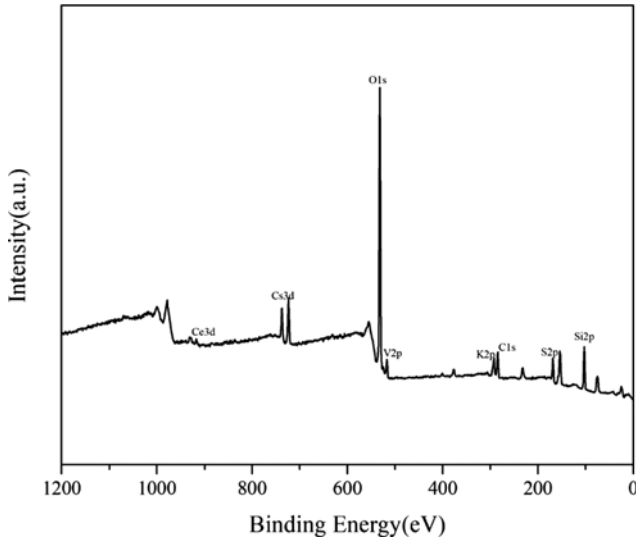

Fig. 10. XPS survey spectra of V-K-Cs-Ce catalyst.

dium, the O 1s peak position was a little lower compared with the literatures [43,44].

Fig. 11 shows the high resolution spectrum of Cs, V and Ce. There are two prominent peaks at 724.0 eV and 738.0 eV in Fig. 11(a), which corresponds to Cs $3d_{5/2}$ and Cs $3d_{3/2}$ core level peaks, respectively [45]. The binding energies of elemental Cs were reported at 726.0 eV (Cs $3d_{5/2}$) and 739.9 eV (Cs $3d_{3/2}$), and the significant shift (~2 eV) of the Cs 3d core level peaks in the catalyst with respect to the corresponding elemental positions clearly indicates the presence of Cs in the bonded form [46]. According to the literature data, the observed Cs 3d core level binding energies (724.0 eV and 738.0 eV) can be for cesium sulfate (Cs_2SO_4) compounds [47].

Fig. 11(b) shows the binding energy of V $2p_{3/2}$ and V $2p_{1/2}$ at 517.5 eV and 524.7 eV, respectively, which are characteristic of at V^{5+} in the catalyst, and peaks of the lower oxidation state of vanadium V^{4+} (516.4 eV) and V^{3+} (515.5 eV) were not detected. These results are in good agreement with those in the literature [48,49]. The low percentage of V^{4+} and V^{3+} on this sample may result from the more available oxygen and the higher stability of V^{5+} after the addition of cerium.

The Ce 3d high-resolution XPS spectra of V-K-Cs-Ce catalyst are shown in Fig. 11(c). The bands of Ce $3d_{3/2}$ (882.2 eV), Ce $3d_{3/2}$ (887.4 eV), Ce $3d_{3/2}$ (893.4 eV), Ce $3d_{5/2}$ (901.3 eV) and Ce $3d_{5/2}$ (907.4 eV) can be attributed to surface Ce^{4+}, whereas Ce $3d_{3/2}$ (884.9 eV) and Ce $3d_{5/2}$ (904.4 eV) correspond to surface Ce^{3+} [11,50-52]. Ce^{3+} can lead to the formation of unsaturated chemical bonds and oxygen vacancies, thus promoting the oxidation of SO_2 to SO_3 especially at low temperatures. After a series of calculations, the mass ratio of CeO_2 on the surface of the catalysts is 3.4 wt%, as some CeO_2 might enter into the channels of diatomite. This speculation has been verified in a further step by the experiments above, especially by BET analysis and SEM.

CONCLUSION

V_2O_5 catalysts promoted with different composition of Cs_2SO_4

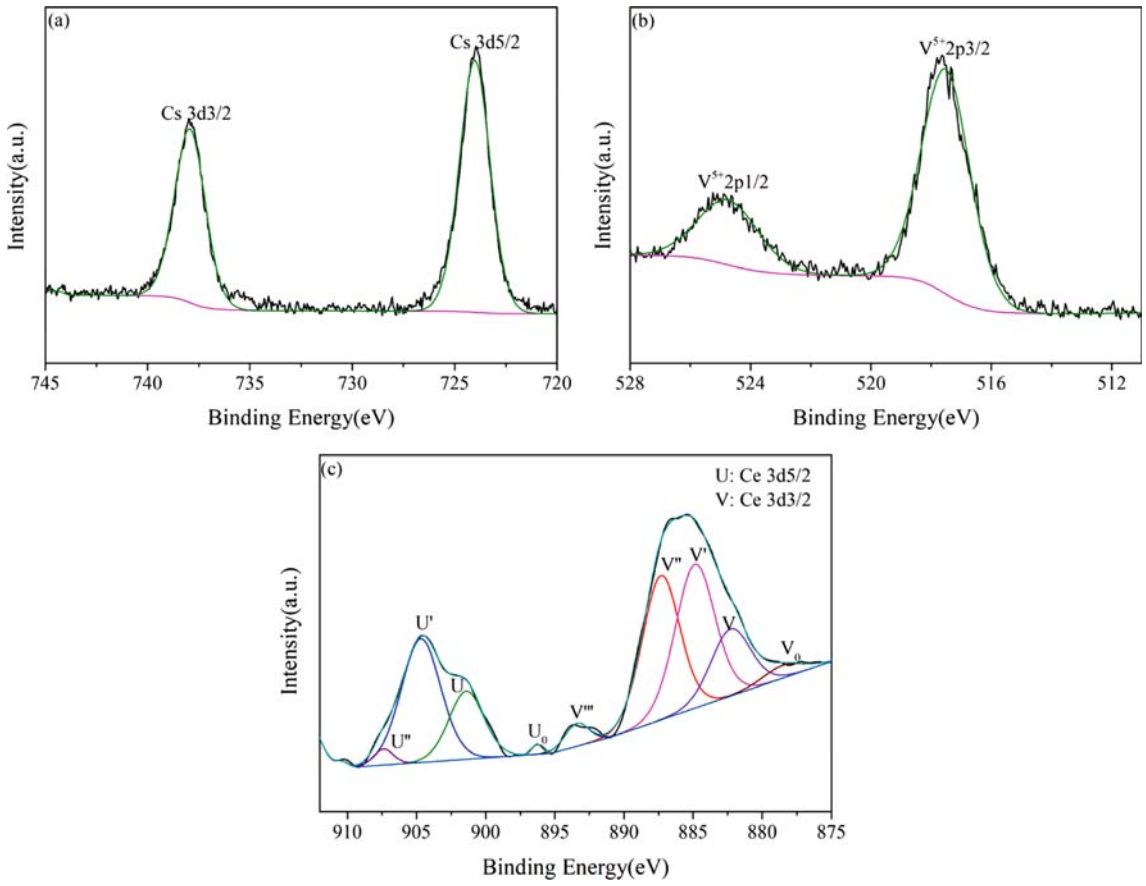

Fig. 11. High resolution spectrum of Cs, V and Ce in V-K-Cs-Ce catalyst.

and CeO_2 were studied for oxidation of SO_2. The results show that V-K-Cs-Ce catalyst has superior catalytic performance in terms of low temperature activity, thermal stability and SO_2 oxidation efficiency. Also, the ignition temperature of the modified catalyst is 340 °C, which is 80 and 40 °C lower than that of commercial vanadium catalyst and cesium vanadium catalyst commonly used in sulfuric acid preparation. Therefore, the V-K-Cs-Ce catalyst is well suited for the oxidation of sulfur dioxide and will hopefully shorten the existing process flow of sulfuric acid preparation.

The positive effects of the modified catalyst on catalytic activity arise from the formation of $CeVO_4$ and CeO_2, and the existence of these crystalline phases can be confirmed by FT-IR, Raman and XRD analysis. $CeVO_4$ and CeO_2 play an important role in redox reaction at low temperature and can increase the available oxygen for the redox reaction. Besides, adding a certain amount of ceria can promote the formation of pyrosulfate and improve the textural properties of catalysts, which is conducive to improving the catalytic activity. Finally, it was found that the formation of inactive phases $KV(SO_4)_2$ and catalytically inactive V^{IV} complex species is minimum in V-K-Cs-Ce catalyst during SO_2 oxidation.

ACKNOWLEDGEMENTS

This work was supported by the National Key R & D Program of China (2017YFC0210203-4).

REFERENCES

1. S. Koutsopoulos, S. B. Rasmussen, K. M. Eriksen and R. Fehrmann, *Appl. Catal. A: Gen.*, **306**, 142 (2006).
2. S. G. Masters, K. M. Eriksen and R. Fehrmann, *J. Mol. Catal. A: Chem.*, **120**, 227 (1997).
3. M. J. King, W. G. Davenport and M. S. Moats, Sulfuric Acid Manufacture, Elsevier, Oxford (2013).
4. U. Bentrup, A. Martin and G.-U. Wolf, *Thermochim. Acta*, **398**, 131 (2003).
5. F. J. Doering, H. K. Yuen, P. A. Berger and M. L. Unland, *J. Catal.*, **104**, 186 (1987).
6. I. Giakoumelou, V. Parvulescu and S. Boghosian, *J. Catal.*, **225**, 337 (2004).
7. A. Wingen, N. Anastasievič, A. Hollnagel, D. Werner and F. Schüth, *J. Catal.*, **193**, 248 (2000).
8. C. L. Chen and H. S. Weng, *Appl. Catal. B: Environ.*, **55**, 115 (2005).
9. Z. X. Zhou, L. N. Wang, Z. Y. Li, S. G. He and T. M. Ma, *J. Phys. Chem. A*, **120**, 3843 (2016).
10. F. Xu, K. Cheng, Y. Yu and S. Mu, *Electrochim. Acta*, **229**, 253 (2017).
11. M. Mazidi, R. M. Behbahani and A. Fazeli, *Appl. Catal. B: Environ.*, **209**, 190 (2017).
12. Y. Mathieu, M. Soulard, J. Patarin and M. Molière, *Fuel Process. Technol.*, **99**, 35 (2012).
13. W. Jiang and B. Liang, *Appl. Catal. A: Gen.*, **311**, 1 (2006).

14. Test method of activity for oxidizing sulphuric dioxide into sulphuric acid catalyst, Chemical industry standard of P.R.C, HG/T 2089-2007.
15. N. Fang, Y. Ding, C. Liu and Z. Chen, *Ceram. Int.*, **44**, 12363 (2018).
16. L. Li, Y. Song, B. Jiang, K. Wang and Q. Zhang, *Energy*, **131**, 58 (2017).
17. F. Meshkani and M. Rezaei, *Int. J. Hydrogen Energy*, **39**, 18302 (2014).
18. Q. Mu and Y. Wang, *J. Alloys Compd.*, **509**, 396 (2011).
19. S. K. Padmanabhan, S. Pal, E. Ul Haq and A. Licciulli, *Appl. Catal. A: Gen.*, **485**, 157 (2014).
20. Y. Mu, M. Cui, S. Q. Zhang, J. Zhao, C. G. Meng and Q. Sun, *Micropor. Mesopor. Mater.*, **267**, 203 (2018).
21. M. Bensitel, O. Saur, J. C. Lavalley and B. A. Morrow, *Mater. Chem. Phys.*, **19**, 147 (1988).
22. M. Ksibi, E. Elaloui, A. Houas and N. Moussa, *Appl. Surf. Sci.*, **220**, 105 (2003).
23. Y. Lu, Z. Zhang, Y. Li and W. Liao, *J. Rare Earth.*, **35**, 34 (2017).
24. M. Kurian and C. Kunjachan, *J. Environ. Chem. Eng.*, **4**, 1359 (2016).
25. J. Liu, Z. Zhao, C. Xu, A. Duan and G. Jiang, *J. Rare Earth.*, **28**, 198 (2010).
26. M. F. R. Fouda, H. I. Saleh, M. M. Abd-Elzaher and R. S. Amin, *Appl. Catal. A: Gen.*, **223**, 11 (2002).
27. I. Giakoumelou, R. M. Caraba, V. I. Parvulescu and S. Boghosian, *Catal. Lett.*, **78**, 209 (2002).
28. A. Christodoulakis and S. Boghosian, *J. Catal.*, **215**, 139 (2003).
29. P. Kumar, B. Ahmad, F. Chand and K. Asokan, *Appl. Surf. Sci.*, **452**, 217 (2018).
30. U. O. Krasovec, B. Orel, A. Surca, N. Bukovec and R. Reisfeld, *Solid State Ionics*, **118**, 195 (1999).
31. C. M. Chanquía, A. L. Cánepa, E. L. Winkler, E. Rodríguez-Castellón, S. G. Casuscelli and G. A. Eimer, *Mater. Chem. Phys.*, **175**, 172 (2016).
32. O. B. Lapina, B. S. Bal'zhinimaev, S. Boghosian, K. M. Eriksen and R. Fehrmann, *Catal. Today*, **51**, 469 (1999).
33. M. V. Bosco, M. A. Bañares, M. V. Martínez-Huerta, A. L. Bonivardi and S. E. Collins, *J. Mol. Catal. A: Chem.*, **408**, 75 (2015).
34. V. I. Parvulescu, C. Paun, V. Parvulescu, M. Alifanti, I. Giakoumelou, S. Boghosian, S. B. Rasmussen, K. M. Eriksen and R. Fehrmann, *J. Catal.*, **225**, 24 (2004).
35. S. Boghosian, F. Borup and A. Chrissanthopoulos, *Catal. Lett.*, **48**, 145 (1997).
36. S. Boghosian, A. Chrissanthopoulos and R. Fehrmann, *J. Phys. Chem. B*, **106**, 49 (2002).
37. N. Inchaurrondo, J. Font, C. P. Ramos and P. Haure, *Appl. Catal. B: Environ.*, **181**, 481 (2016).
38. M. Sljivic, I. Smiciklas, S. Pejanovic and I. Plecas, *Appl. Clay Sci.*, **43**, 33 (2009).
39. R. Zheng, Z. Ren, H. Gao, A. Zhang and Z. Bian, *J. Alloys Compd.*, **757**, 364 (2018).
40. K. Jabbour, N. El Hassan, A. Davidson, P. Massiani and S. Casale, *Chem. Eng. J.*, **264**, 351 (2015).
41. P. Z. Lv, C. Z. Liu and Z. H. Rao, *Renew. Sust. Energy Rev.*, **68**, 707 (2017).
42. F. R. Lamastra, S. Mori, V. Cherubini, M. Scarselli and F. Nanni, *Mater. Chem. Phys.*, **194**, 253 (2017).
43. P. Zhu, Y. Chen, M. Duan, M. Liu and P. Zou, *Powder Technol.*, **336**, 230 (2018).
44. Y. Chen, Q. Wu, C. Zhou and Q. Jin, *Adv. Powder Technol.*, **29**, 106 (2018).
45. M. Pilarski, R. Marschall, S. Gross and M. Wark, *Appl. Catal. B: Environ.*, **227**, 349 (2018).
46. P. K. Narayanam, A. Jishnu and K. Sankaran, *Colloids Surf., A*, **539**, 416 (2018).
47. M. Wahlqvist, A. Shchukarev and J. Electron. *Spectrosc. Relat. Phenom.*, **156-158**, 310 (2007).
48. C. Wang, Z. Chen, X. Yao, W. Jiang, M. Zhang, H. Li, H. Liu, W. Zhu and H. Li, *RSC Adv.*, **7**, 39383 (2017).
49. L. Rivoira, M. L. Martínez, O. Anunziata and A. Beltramone, *Micropor. Mesopor. Mater.*, **254**, 96 (2017).
50. G. Seong, M. Dejhosseini and T. Adschiri, *Appl. Catal. A: Gen.*, **550**, 284 (2018).
51. G. K. Reddy, P. Boolchand and P. G. Smirniotis, *J. Catal.*, **282**, 258 (2011).
52. R. Peng, S. Li, X. Sun, Q. Ren, L. Chen, M. Fu, J. Wu and D. Ye, *Appl. Catal. B: Environ.*, **220**, 462 (2018).